UNCLASSIFIED

AD 275 463

Reproduced
by the

ARMED SERVICES TECHNICAL INFORMATION AGENCY
ARLINGTON HALL STATION
ARLINGTON 12, VIRGINIA

UNCLASSIFIED

DISCLAIMER NOTICE

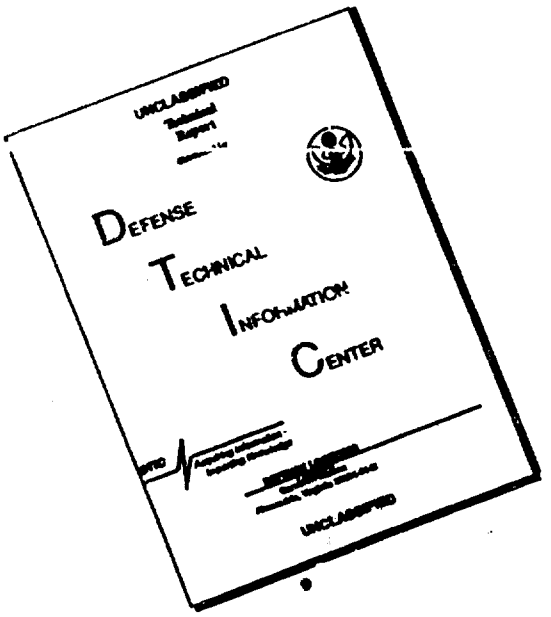

THIS DOCUMENT IS BEST QUALITY AVAILABLE. THE COPY FURNISHED TO DTIC CONTAINED A SIGNIFICANT NUMBER OF PAGES WHICH DO NOT REPRODUCE LEGIBLY.

NOTICE: When government or other drawings, specifications or other data are used for any purpose other than in connection with a definitely related government procurement operation, the U. S. Government thereby incurs no responsibility, nor any obligation whatsoever; and the fact that the Government may have formulated, furnished, or in any way supplied the said drawings, specifications, or other data is not to be regarded by implication or otherwise as in any manner licensing the holder or any other person or corporation, or conveying any rights or permission to manufacture, use or sell any patented invention that may in any way be related thereto.

AD 275463
CATALOGED BY ASTIA
AS AD NO.

SECTION T

THE JOHNS HOPKINS UNIVERSITY
APPLIED PHYSICS LABORATORY
8621 Georgia Avenue, Silver Spring, Maryland

CM-1010

Operating under Contract NOrd 7386 with the Bureau of Naval Weapons, Department of the Navy

Copy No. 15

SECONDARY GAS INJECTION IN A CONICAL ROCKET NOZZLE

I. EFFECT OF ORIFICE DIAMETER AND MOLECULAR WEIGHT OF INJECTANT

MAY

by

R. E. Walker, A. R. Stone, and M. Shander

Released to ASTIA by the Bureau of
without restriction.
NAVAL WEAPONS

February 1962

CM-1010
February 1962

Secondary Gas Injection in a Conical Rocket Nozzle

I. Effect of Orifice Diameter and Molecular Weight of Injectant

by
R. E. Walker, A. R. Stone, and M. Shandor

THE JOHNS HOPKINS UNIVERSITY
APPLIED PHYSICS LABORATORY
8621 GEORGIA AVENUE SILVER SPRING MARYLAND

The Johns Hopkins University
APPLIED PHYSICS LABORATORY
Silver Spring, Maryland

ABSTRACT

Data are presented on interference forces resulting when a gas at ambient temperature is laterally injected through a single circular orifice in the conical portion of a rocket nozzle into hot supersonic propellent gases. Variables examined are (a) injectant orifice size and associated pressure ratio change and (b) effect of injectant molecular weight and specific heat ratio. Other parameters remain essentially constant during these tests. It is shown that simple theoretical arguments can predict relative effects of intrinsic injectant properties, but that pressure ratio effects are not adequately described. It is also shown that effectiveness of secondary injection depends on injectant orifice size, which has not been treated in any theoretical models.

The Johns Hopkins University
APPLIED PHYSICS LABORATORY
Silver Spring, Maryland

TABLE OF CONTENTS

The Johns Hopkins University
APPLIED PHYSICS LABORATORY
Silver Spring, Maryland

LIST OF ILLUSTRATIONS

The Johns Hopkins University
APPLIED PHYSICS LABORATORY
Silver Spring, Maryland

LIST OF TABLES

LIST OF SYMBOLS

A_j	=	Jet orifice area
A_t	=	Nozzle throat area
A_1	=	Nozzle area at point of injection
C_D	=	Discharge coefficient of orifice assuming sonic flow
d_j	=	Orifice diameter
F_N	=	Side force due to secondary injection
F	=	Axial thrust of motor
I_s	=	$F_N/\dot{W}_j$, Effective specific impulse of injectant
I_s^*	=	Specific impulse of vacuum-exhausted sonic jet of injectant, Eq. (7)
M_1	=	Mach number of nozzle flow at point of injection
$M_{j\infty}$	=	Mach number of jet gases after expanding to freestream pressure
$\mathcal{M}$	=	Molecular weight of propellent gases
$\mathcal{M}_j$	=	Molecular weight of injectant
$\overset{o}{m}_j(M_{j\infty})$	=	Mass flow function defined by Eq. (5)
P_1	=	Static pressure of nozzle flow at point of injection
P_2	=	Static pressure behind induced oblique shock wave
P_o	=	Stagnation pressure of propellent gases
P_{oj}	=	Stagnation pressure of injectant
P_j	=	Static pressure of injectant at orifice

T_o = Stagnation temperature of propellant

T_{oj} = Stagnation temperature of injectant

$\dot{W}_j$ = Mass flow rate of injectant

$\dot{W}$ = Mass flow rate of propellant

γ = Specific heat ratio of propellant

γ_j = Specific heat ratio of injectant

α = Conical nozzle half angle, 15°

The Johns Hopkins University
APPLIED PHYSICS LABORATORY
Silver Spring, Maryland

SECONDARY GAS INJECTION IN A CONICAL ROCKET NOZZLE
I. Effect of Orifice Diameter and Molecular Weight of Injectant[1]

I. SUMMARY AND CONCLUSIONS

This report is the first in a series dealing with an experimental study of thrust vector control using gaseous secondary injection. For this study, the main propellant was a hot gas (catalytically decomposed H_2O_2); a variety of gases (CO_2, N_2, Ar, 0.8 He + 0.2 Ar, He, and H_2) at ambient temperature was used as the injectant. A conical convergent-conical divergent exhaust nozzle was used, with injection normal to the nozzle axis at a fixed point in the divergent portion of the nozzle.

A variety of circular orifice diameters (0.180, 0.125, 0.089, 0.0625, and 0.04 inches) was examined. The side force developed by secondary injection was measured directly with a force transducer; the data are reported as specific impulse ratio or "amplification factor" obtained by dividing the measured effective specific impulse of the injectant by the specific impulse of the injectant for sonic flow into a vacuum.

As the orifice diameter was varied (with CO_2 injectant), low-pressure injection was critically examined. The results showed that for a particular orifice size the

[1]This work was sponsored by the Special Projects Office, Bureau of Naval Weapons.

amplification factor has a maximum at or near the transition from sonic to subsonic injection. Performance does not increase indefinitely for decreasing pressure ratio across the orifice, as might be construed from simple linear supersonic flow theory. Significant effects of orifice size on the specific impulse ratio were observed: For a fixed pressure ratio across the orifice, performance increases with decreasing orifice size.

Subsonic injection data aided in estimating the strength of the shock wave induced in the supersonic flow. These data have shown indirectly that shock wave strength increases to a limiting value close to that required for shock wave-turbulent boundary layer separation.

Performance of several inert gas injectants with differing molecular weights and specific heat ratios correlated well with a parameter suggested by linear supersonic flow theory. One potentially reactive injectant (H_2) was used; its data correlated well with the inert gas data and suggest that essentially no reaction occurred in the nozzle between the injectant and propellant.

Additional experiments designed to measure the effects of other parameters (such as injectant temperature, motor temperature and pressure, and injection and nozzle geometry) are desirable to establish appropriate theoretical avenues. Some of these experiments are presently in progress at this Laboratory.

II. BACKGROUND

Recent advances in solid rocket propellant technology resulting in higher flame temperatures and multiphase flow have increased the desirability of thrust vector control methods that do not require exposing moving material parts to propellant exhaust products. For this reason, other methods of deflecting the supersonic nozzle flow are being examined. Secondary injection is one method that has received considerable attention. This technique utilizes the forces developed on the wall of the divergent portion of the rocket exhaust nozzle by lateral injection of a fluid (gas or liquid) into the supersonic propellant gases. In addition to the usual jet reaction, local high pressures associated with an induced shock wave "amplify" the jet reaction. The first experiments on secondary injection were reported by Hausmann (1)[2] and demonstrated that the shock-induced reaction associated with an air jet directed into supersonic air (both gases at ambient temperature) could for certain conditions be as large as the jet reaction. The nature of this shock-induced reaction and how it depends upon the mainstream and injectant properties has since been the subject of considerable study, mostly experimental. Several experiments have been reported for jet-interference phenomena on simple aerodynamic surfaces (2-6), on the external surfaces of simple missile configurations (7-9), and on the internal surfaces of rocket nozzles (secondary injection) (10-16). Most of these reports

[2]Numbers in parentheses indicate references at end of paper. References are listed on pages 41, 42, and 43.

deal with ambient temperature air-air interaction. Because of the complexity of the problem, analytical descriptions have been quite limited. For gas injection, two qualitatively-correct basic descriptions have been useful (8, 17-19), but refinements are desirable.

This report presents the results of experiments performed at this Laboratory on secondary gas injection into hot supersonic propellant flow in a small rocket motor. Data on the effects of injectant gas properties and injectant orifice size have been obtained; motor operating conditions, nozzle geometry, and injectant location have been kept fixed. Future experiments involving temperature effects, nozzle geometry, point of injection, and mainstream properties are planned.

III. DESCRIPTION OF EXPERIMENTAL APPARATUS AND TESTING PROCEDURE

Apparatus

The data presented in this report were obtained with a small research rocket motor and nozzle, sketched in Fig. 1. The working fluid was provided by catalytic decomposition of 90 per cent hydrogen peroxide liquid[3] at a nominal motor chamber pressure of 400 psia. The products of decomposition were 29.2 per cent mole fraction of oxygen and 70.8 per cent mole fraction of water vapor, with a specific heat ratio of 1.266 (20). Average propellant exhaust temperature, measured with an uncalibrated iron-constantan thermocouple, was 1845°R (Rankine), with a maximum spread of 1830-1865°R. This temperature is slightly higher than the theoretical adiabatic decomposition temperature, 1825°R (20).

Some motor, nozzle, and injectant properties are listed in Table I. Attempts to measure the liquid propellant flow rate $\dot{W}$ were unsuccessful. It was therefore necessary to rely upon motor chamber pressure P_o and temperature T_o(=1845°R), geometrical area of the nozzle throat A_t(=0.196 in^2), and isentropic flow relations to compute propellant flow rate, theoretically, $\dot{W} = 0.00280\ P_o$ where $\dot{W}$ is in lb/sec and P_o is in psia.

The average thrust coefficient C_F for motor chamber pressure of about 400 psia has been found experimentally to be 1.42, which is somewhat below the theoretical value of 1.46

---

[3]Supplied by Becco Chemical Division, Food Machinery and Chemical Corporation.

(based upon conical isentropic nozzle flow and area ratio for P_o = 400 psia, and an atmospheric pressure of 14.7 psia). Axial thrust F for these experiments can be closely computed from $F = C_F A_t P_o \approx 0.278\ P_o$, with F in lb and P_o in psia.

Injectant gases were obtained from standard compressed gas containers.[4] A maximum injectant pressure of about 500 psia was used for carbon dioxide and about 1000 psia for the other gases; injectant gas temperature was ambient, nominally 70°F. The injectant gas flow rate was metered through a standard ASME sharp-edged orifice flowmeter calibrated with CO_2 by timed discharge into a calibrated volume. Molecular weight and compressibility corrections were made in the usual manner when other injectant gases were used. Evaluation of the discharge coefficient of the injectant orifice in the nozzle wall by using a combination of this metered flow rate $\dot{w}_j$, measured jet total pressure P_{oj}, total temperature T_{oj} geometric orifice area $A_j (=\pi d_j^2/4)$, and isentropic flow relations provided a compatibility check for several measured parameters.

Figure 2 shows the general setup of the apparatus. The motor is mounted on the periphery of and in line with the axis of a drum, the axle of which is mounted in antifriction bearings that permit simultaneous rotation and axial motion. The drum floats in water to reduce bearing load. Force transducers measure axial motor thrust and turning moment developed by secondary injection or by motor trim misalignment. Propellant and injectant go to the nozzle through relatively long rigid lines which by test were found to introduce fixed

---

[4] Carbon dioxide for these experiments was supplied by Pure Carbonic Company. All other gases were supplied by Southern Oxygen Company.

spring constants superimposed on the elastic constants of the force transducers. Transducer calibrations are obtained after or during each day of operation with the transducers in place.

Most pressure measurements were made with a variety of electrical pressure transducers which had been periodically calibrated with bourdon element test gauges. The gauges had in turn been calibrated against a standard dead weight tester. Where possible, all transducers were excited from a common monitored supply voltage, and observed variations in excitation voltage were included in the data analysis. Temperature measurements were made with uncalibrated iron-constantan thermocouples. Appropriately attenuated transducer and thermocouple outputs were recorded on four 0-1 mv, 10-inch Westronix strip-chart recorders either continuously or through a dual 6-point data sampler which permits more than one bit of information per recorder channel.

Testing Procedure

Because there had been some transients, the following operating sequence was adopted:

(1) One complete data sampling sequence (≈12 sec), without propellant or injectant flow, to establish transducer and recorder zeros. No special effort was made to preadjust transducer outputs to zero.

(2) Propellant-on--injectant-off sequence to determine thrust misalignment (motor trim).

(3) Propellant-on--injectant-on to measure secondary injection effects.

(4) Repeat of (2.) to determine trim change, if any.

(5) Repeat of (1) to determine transducer zero shift, if any.

This procedure permits all bits of information to be extrapolated and evaluated at a common time.

IV. EXPERIMENTAL RESULTS

Data were obtained on the separate effects of

(1) injectant orifice size, and

(2) the effect of injectant gas type.

Only injection normal to the nozzle axis was examined. The motor chamber pressure was kept at the experimental maximum value of about 400 psia. The propellent gases had a stagnation temperature close to 1845°R.

The injectant port, a single circular orifice, was located at the point in the conical expansion nozzle where the Mach number, M_1, was 2.34. This Mach number was determined both by the experimentally measured pressure ratio $P_1/P_o = 0.0730$ and the geometrical area ratio $A_1/A_t = 2.597$. The static pressure of the undisturbed supersonic flow at the injection point was nominally 30 psia. The exit Mach number of the nozzle M_3 was computed from the geometrical area ratio A_3/A_t to be 2.83. The exhaust gases were slightly overexpanded at the nozzle exit, $P_3 = 12.8$ psia. No attempt was made to reduce P_o in order to examine secondary-injection-induced separation effects.

In the study of the effects of orifice size, carbon dioxide at ambient temperature (nominally 70°F) was selected as the injectant and the orifice diameter d_j was varied from 0.0625 to 0.180 inches. Changes in the orifice size were accomplished by simply "drilling out" the just-tested orifice. This practice gives a kind of thick, square-edged orifice

whose discharge coefficient can be expected to depend strongly on Reynolds number and pressure ratio across the orifice. The variation in this pressure ratio P_{oj}/P_1 brought about by varying the jet mass flow was sufficient to give both subsonic and sonic flow through the orifice ($1.4 < P_{oj}/P_1 < 12$). In retrospect, carbon dioxide was a poor choice for a working gas since, at the pressures and temperatures involved, significant compressibility effects were encountered. (For example, at 500 psia and 70°F the compressibility factor for carbon dioxide is 0.79 and represents a considerable and measurable departure from ideal gas behavior). Compressibility effects were taken into account when evaluating the orifice discharge coefficient by using a linearized treatment given by Eggers (21) for a calorically perfect but thermally imperfect gas. Separate experiments were performed to establish the validity of using this linearized analysis. No other compressibility effect corrections were made to the data.

A detailed listing of the experimental data is provided in Table II. A summary plot of the data pertaining to effect of orifice size is provided in Fig. 3, where the normalized specific impulse I_s/I_s^* and sonic discharge coefficient C_D are plotted as a function of jet pressure ratio P_{oj}/P_1.

The effective specific impulse I_s is obtained by dividing the force normal to the motor axis F_N by the measured jet mass flow $\dot{W}_j$. I_s^* is the specific impulse of a sonic jet of the injectant exhausting into a vacuum. I_s/I_s^*, therefore, represents an amplification factor for secondary injection.

The sonic discharge coefficient C_D is obtained by dividing the measured jet mass flow by a theoretical value based upon sonic isentropic flow, the geometrical area of the orifice, and measured values of P_{oj} and T_{oj}. The breaking

away of C_D from a constant value near unity is interpreted to be a transition from sonic to subsonic injection. As seen in Fig. 3, the knee of the C_D curve occurs at a value of P_{oj}/P_1 larger than the critical pressure ratio for jet flow without supersonic cross-flow interference. This results from higher effective back pressures brought about by the induced shock wave. Note also that the I_s/I_s^* curve tends to peak at or near this transition point and does not exhibit a monotonically increasing behavior for a decreasing P_{oj}/P_1, as might be inferred from simple theory discussed later.

Finally, the strong dependence of secondary injection effectiveness upon orifice size should be recognized. The variation in d_j examined here exceeds that studied by others and the consequence of varying d_j has not been pointed out before.

Several gases have been used to investigate the effects of injectant molecular weight M_j and specific heat ratio γ_j; the gases used are listed in Table III. All of these injectants are inert with the exception of H_2 which, in principle, could react with the hot O_2-H_2O propellant exhaust products. As will be seen later, there was no evidence of combustion. The observed failure to ignite may be attributed to the low exhaust temperature, which presumably is inadequate to support supersonic combustion (22). The detailed data are included in Table II and a summary plot is given in Fig. 4. Ambient temperature injection through a 0.0625-inch diameter orifice has been used throughout. For reasons to be presented later, a modified correlating parameter, $(1 + \gamma_j)I_s/I_s^*$, has been used in Fig. 4 where, with the exception of the argon data, quite a good correlation has been provided. So far, all attempts to locate errors in the argon results have been futile.

The reason, if any, for this disparity has not been reconciled. Characteristics associated with subsonic and sonic injection are similar to the data presented in Fig. 3.

A series of experiments was undertaken to determine the gain in axial motor thrust as a result of secondary injection. Ambient temperature injection of CO_2 through a 0.180-inch-diameter orifice was used. The axial thrust change, ΔF, was measured as a function of $\dot{W}_j$ and F_N. The ratio $\Delta F/(F_N \tan \alpha)$ was computed and found to be 1.30 ± 0.09, which was independent of $\dot{W}_j$ within the accuracy of the experiment. Since the pressure rise associated with secondary injection is distributed about the circumference of the nozzle and F_N is the integrated force component in the plane containing the orifice and nozzle centerlines, a value of $\Delta F/(F_N \tan \alpha)$ larger than unity (flat plate value) is to be expected.

V. THEORETICAL FOUNDATION

The foundation for the series of tests reported here is a modified theoretical model given by Vinson, Amick, and Liepman (8). This model has been found (in general) to be in qualitative agreement with the bulk of experimental data. Because of its simplicity and flexibility it served as a guide in selecting experimental parameters. This two-dimensional "weak" jet model assumes that the injected gases expand isentropically and without mixing to form a step-like obstacle to the supersonic flow. An oblique shock wave which causes flow separation followed by a Prandtl-Meyer expansion is introduced to provide proper flow deflection of the mainstream. (Fig. 5.)

The net force acting upon the wall as a result of the injected gases for this model can be simply computed from linearized supersonic flow theory (which should be valid if mainstream deflections are not too large) providing one integrates along the control surface indicated in Fig. 5. According to linearized supersonic flow theory (23), the pressure coefficient $C_p = 2(P - P_1)/P_1 \gamma M_1^2$ is given as

$$C_p = \frac{2}{\sqrt{M_1^2 - 1}} \left(\frac{dy}{dx}\right)_{str} \qquad (1)$$

where $(dy/dx)_{str}$ is the slope of the streamline. Integration along the streamline that divides the injectant and mainstream gives for the total force normal to the mainstream flow direction (per unit width)

$$F_N = \int_{-\infty}^{+\infty} (P - P_1)_{str} dx = \frac{P_1 \gamma M_1^2 y_\infty}{\sqrt{M_1^2 - 1}} \qquad (2)$$

where y_∞ is the asymptotic displacement of the streamline from the wall necessary to accommodate the injected gases.

The result given by Eq. (2) has been used by Vinson, et al (8) to compute the induced reaction which is then added to the jet reaction to obtain the total interference force. Such a procedure may be approximately correct for orifices located near the trailing edge of the body, but within the restrictions of the linear theory Eq. (2) alone will give the total reaction for a body of infinite length.

For a finite-sized orifice, a pseudo two-dimensional analysis would give

$$F_N = P_1 A_\infty \gamma M_1^2 / (M_1^2 - 1)^{1/2} \qquad (3)$$

where A_∞ is now the asymptotic area through which the injectant passes after being expanded to P_1. Isentropic expansion

was assumed by Vinson, et al. The $P_1 A_\infty$ product can be related to the injectant flow rate of $\dot{W}_j$ by

$$P_1 A_\infty = \dot{W}_j \, (T_{oj})^{1/2} / \overset{o}{m}_j \, (M_{j\infty}) \tag{4}$$

where T_{oj} is the stagnation temperature of the injectant and $\overset{o}{m}_j \, (M_{j\infty})$ is the mass flow function defined as

$$\overset{o}{m}_j \, (M_{j\infty}) = M_{j\infty} \left[\left(\frac{\gamma_j \mathcal{M}_j}{R} \right) \left(1 + \frac{\gamma_j - 1}{2} M_{j\infty}^2 \right) \right]^{1/2} \tag{5}$$

where $\mathcal{M}_j$ is the injectant molecular weight and R is the universal gas constant.

Substituting Eq. (4) into Eq. (3) gives for the effective specific impulse of the injectant

$$I_s = \frac{F_N}{\dot{W}_j} = \frac{(T_{oj})^{1/2}}{\overset{o}{m}_j (M_{j\infty})} \cdot \frac{\gamma M_1^2}{(M_i^2 \cdot 1)^{1/2}} \tag{6}$$

If we normalize Eq. (6) by dividing by the specific impulse of the vacuum exhausted sonic jet of the injectant,

$$I_s^* = (1 + \gamma_j)(T_{oj})^{1/2} / \overset{o}{m}_j (1). \tag{7}$$

we obtain

$$(1 + \gamma_j)\frac{I_s}{I_s^*} = \frac{\overset{o}{m}_j(1)}{\overset{o}{m}_j(M_{j\infty})}\frac{\gamma M_1^2}{(M_1^2 - 1)^{1/2}} \tag{8}$$

$$= \frac{\gamma M_1^2}{(M_1^2 - 1)^{1/2}}\left\{\frac{1 + \gamma_j}{M_{j\infty}^2[2+(\gamma_j - 1)M_{j\infty}^2]}\right\}^{1/2}$$

Although Eq. (8) cannot be expected to apply in detail to the experiments in question, some general or qualitative interpretations can be deduced that will aid in analyzing or correlating the data and in making predictions as to secondary injection performance. Some of these features are:

(1) As long as one assumes an adiabatic process for the injected gases, the parameter $(1 + \gamma_j)I_s/I_s^*$ is independent of $\mathcal{M}_j$ and T_{oj} and essentially independent of γ_j.

(2) Within the restrictions of the linear theory, the extent of boundary layer separation does not affect the magnitude of the interference force resulting from secondary injection. However, the pressure rise associated with the induced shock (which by postulate gives rise to the separated flow) can be expected to influence the thermodynamic process of the injected gases, i.e the extent of total pressure loss (if any)

as a result of possible shock formation in the jet gases.

(3) The mainstream values for γ and (more significantly) M_1 appear in Eq. (8) and can be expected to influence secondary injection performance, whereas the molecular weight $\mathcal{M}$ and temperature T_0 of the mainstream do not appear to be significant parameters.

(4) The pressure ratio P_{oj}/P_1 will determine $M_{j\infty}$ for any given mainstream conditions; however, $M_{j\infty}$ cannot be calculated a priori since the thermodynamic process of the jet gases can be expected to depend upon the separated flow conditions. Since $M_{j\infty}$ will become small as P_{oj}/P_1 approaches unity, I_s/I_s^* should increase with decreasing P_{oj}/P_1 and, in fact, will diverge at $M_{j\infty} = 0$.

Because of the several restrictions on this theory, it cannot be used directly for the analysis of secondary gas injection in rocket nozzle flows. The qualitative arguments presented above nevertheless can still be expected to be valid

VI. DISCUSSION OF THE DATA

The data presented in Fig. 3 on the effect of injectant orifice diameter were taken in order to examine the theoretical postulate that the effectiveness of secondary injection should increase as the P_{oj}/P_1 ratio is decreased. This diverging characteristic has been observed in a number of experiments reported by others, but the low pressure ratio extremes have not been critically examined. The sonic injection data presented in Fig. 3 show the characteristic decline that has also been observed by others in secondary injection performance for increasing P_{oj}/P_1 ratios.

However, this trend does not prevail for subsonic injection; it has been observed that as the jet becomes subsonic (as indicated by the knee in the discharge coefficient curve), performance tends to decrease slightly with decreasing P_{oj}/P_1. The most efficient performance is achieved at or near the transition from sonic to subsonic injection. This behavior is not unique to this experiment (15). It is worthwhile to point out that this transition pressure ratio $(P_{oj}/P_1)_{tr}$ is compatible with an effective jet back pressure that will give combined "just-choked" jet flow and turbulent boundary layer separation of the mainstream ahead of the port. The pressure rise to give turbulent boundary layer separation for $M_1 = 2.4$ air is approximately $(P_2/P_1)_{sep} = 2.2$ (24). If one assumes that the static pressure at the jet orifice P_j is approximately equal to the pressure in the separated region P_2, then

$$(P_{oj}/P_1)_{tr} = (P_o/P)^*(P_2/P_1)_{sep} = (2.0)(2.2) \quad 4.4$$

which is in reasonable agreement with Fig. 3.

Additional information on the pressure rise associated with the induced shock wave can be obtained from the subsonic injection data in the following manner: If one assumes one-dimensional isentropic flow for the jet gases and a discharge coefficient equal to its asymptotic value at large P_{oj}/P_1, the static pressure at the jet orifice P_j can be evaluated from the measured values of $\dot{W}_j$, P_{oj}, T_{oj}, and A_j. In addition, we assume that $P_j \approx P_2$. The results of such calculations for the subsonic CO_2 injection data appear in Fig. 6. For P_{oj}/P_1 less than about 3, the pressure rise P_2/P_1 increases almost linearly with P_{oj}/P_1 (increasing jet flux). For P_{oj}/P_1 greater than about 3, P_2/P_1 tends to level off at approximately a value required to give turbulent boundary layer separation. This would suggest that the induced oblique shock wave is probably attached initially to the leading edge of the orifice, and its strength increases with increase in jet flux until it reaches a limiting pressure rise sufficient to give separation. The shock then detaches from the orifice lip and moves upstream with increasing P_{oj}/P_1. This interpretation is compatible with the theoretical model discussed above.

The theoretical model fails, however, to present even a qualitatively correct interpretation of the subsonic injection data for which it should be most applicable; i.e., it does not predict a decreasing I_s/I_s^* for decreasing P_{oj}/P_1. This characteristic has not been demonstrated for any known theoretical description.

In addition, the strong influence that d_j has upon the effectiveness of secondary gas injection as shown by the data in Fig. 3 had not been established in the reports of other

experiments and was not anticipated. Theory has not been developed to the point of including three-dimensional effects and is of no help in interpreting these data.

It is quite interesting, however, to replot the data of Fig. 3 as I_s/I_s^* versus $\dot{W}_j/\dot{W}$, which is essentially the form frequently used by others to report secondary injection data. Figure 7 is such a graph and shows that all sonic CO_2 injection data correlates rather well. (The subsonic injection data do not correlate on this plot.) The reason for the correlation is not clear since the independent variable $\dot{W}_j/\dot{W}$ suggests a kind of one-dimensional flow not physically plausible or consistent with restriction of the induced oblique-shock pressure rise (approximately) to within the Mach cone emanating from the wall-jet perturbation. Nevertheless, a one-dimensional model with assumed complete mixing of the injectant gases with the supersonic flow has been given by Bonham and Green (25) to establish the relevant parameters for secondary injection. Such an approach fails, however, to predict the effect of variations in injectant molecular weight observed experimentally in this study. It must be concluded that the effect of d_j on secondary gas injection is not well understood and a more comprehensive analytical model would be welcomed.

With the correlation provided in Fig. 5, relative changes in injectant molecular weight and specific heat ratio appear predictable with Eq. (8). Because the H_2 injection data appear to correlate well with other inert gas injection data, it has been concluded that no combustion takes place between the H_2 and the hot H_2O-O_2 exhaust gases. This conclusion is consistent with the research of Chinitz and Gross (22), who reported that combustion between H_2 and heated

supersonic air does not occur below a critical stagnation air temperature of about 2000°F. By inference, the relative effect of changing injectant total temperature can also be predicted, but additional data on this parameter would be desirable. These conclusions unfortunately must be qualified somewhat because of the nonconforming but apparently error-free argon data.

Additional experiments designed to measure the effects of other parameters (such as, T_{oj}, T_o, M_1, P_1, and nozzle geometry) are desirable in order to establish appropriate theoretical evenues. Some of these experiments are presently in progress at this Laboratory.

Table I

Properties of research rocket motor, nozzle, and injectants used in secondary gas injection experiments

Motor		
	Propellant	90% H_2O_2
	Exhaust gas composition	0.708 mole fraction H_2O 0.292 mole fraction O_2
	Thrust coefficient, C_F	1.42
	Pressure, P_o	~ 400 lbs/in^2
	Propellant flow rate, $\dot{W}$	~ 0.84 lbs/sec
	Exhaust gas total temperature, T_o	1845°R
	Specific heat ratio, γ	1.266
	Ambient pressure	atmospheric
Injectant		
	Gas	CO_2, N_2, He, He + Ar, Ar, and H_2
	Injectant pressure, P_{oj}	40-1000 lbs/in^2
	Injectant total temperature, T_{oj}	~70°F
	Injectant port diameter, d_j	0.0625, 0.089, 0.125, 0.180 in.
Nozzle	(Conical, sharp-edged throat)	
	Divergent half angle, α	15 degrees
	Throat diameter, d_t	0.501 inches
	Exit diameter, d_3	1.074 inches
	Nozzle diameter at injectant port, d_1	0.812 inches
	Mach Number at injection plane, M_1	2.34
	Exit Mach Number, M_3	2.83

Table II

Secondary Gas Injection Data

Injectant - CO_2 Orifice Diameter, d_j - 0.180 inches

P_o psia	P_{oj} psia	$\dot{W}_j$ lbm/sec.	F_N lbm.	I_s[a] sec.	P_{oj}/P_1	I_s/I_s*[b]	C_D[c]
393	48.3	0.0058	0.52	86.2	1.57	1.90	0.186
398	52.3	0.0086	0.80	90.7	1.78	2.00	0.238
402	53.3	0.0088	0.84	94.0	1.81	2.08	0.327
410	59.0	0.0120	1.12	92.5	1.97	2.04	0.288
409	63.3	0.0145	1.39	93.2	2.12	2.06	0.331
404	66.7	0.0175	1.54	87.8	2.26	1.94	0.367
406	72.0	0.0207	1.95	92.9	2.43	2.05	0.399
409	75.4	0.0230	2.13	92.6	2.50	2.04	0.428
407	81.1	0.0292	2.61	89.4	2.73	1.97	0.502
406	80.7	0.0288	2.64	89.9	2.74	1.99	0.507
397	91.6	0.0423	3.75	88.2	3.15	1.95	0.648
408	102	0.0554	4.86	88.4	3.43	1.95	0.747
412	110	0.0640	5.53	87.7	3.66	1.94	0.799
393	108	0.0666	5.64	87.1	3.71	1.92	0.835
402	110	0.0658	5.57	83.1	3.73	1.84	0.850
403	131	0.0895	7.39	84.5	4.45	1.87	0.913
413	138	0.0967	7.99	84.8	4.58	1.87	0.944
396	141	0.0991	8.13	84.1	4.86	1.86	0.945

Table II - continued

Injectant - CO_2 Orifice Diameter, d_j - 0.125 inches

P_o psia	P_{oj} psia	$\dot{W}_j$ lbs/sec.	F_N lbs.	I_s[a] sec.	P_{oj}/P_j	I_s/I_s^*[b]	C_D[c]
398	67.0	0.0086	0.82	92.6	2.28	2.04	0.381
397	76.0	0.0130	1.25	94.0	2.58	2.08	0.503
403	86.2	0.0188	1.83	96.3	2.92	2.13	0.638
404	87.8	0.0213	2.03	94.4	2.98	2.08	0.711
404	98.2	0.0256	2.47	95.7	3.28	2.11	0.778
412	105	0.0298	2.93	98.3	3.48	2.17	0.824
404	105	0.0307	3.02	97.2	3.55	2.15	0.853
407	120	0.0379	3.79	100.6	4.01	2.22	0.902
404	142	0.0462	4.47	97.6	4.82	2.15	0.925
408	166	0.0547	5.32	97.9	5.59	2.16	0.938
400	165	0.0553	5.17	94.7	5.60	2.09	0.942
402	187	0.0622	5.85	93.8	6.36	2.07	0.951
403	202	0.0693	6.32	92.8	6.86	2.05	0.953

Table II - continued

Injectant - CO_2 Orifice Diameter, d_j - 0.089 inches

P_o psia	P_{oj} psia	$\dot{W}_j$ lbs/sec.	F_N lbs.	I_s[a] sec.	P_{oj}/P_1	I_s/I_s*[b]	C_D[c]
408	196	0.0316	3.27	103.6	6.57	2.29	0.911
402	201	0.0331	3.30	100.5	6.77	2.22	0.912
401	264	0.0435	4.29	98.6	8.92	2.18	0.915
405	273	0.0439	4.33	98.5	9.2	2.18	0.892
420	326	0.0541	5.25	98.1	11.0	2.17	0.901
397	328	0.0539	5.10	94.6	11.2	2.09	0.905
402	356	0.0581	5.58	95.7	12.1	2.11	0.898
401	358	0.0600	5.70	94.9	12.2	2.10	0.916

Table II - continued

Injectant - CO_2 Orifice Diameter, d_j - 0.0625 inches

P_o psia	P_{oj} psia	$\dot{W}_j$ lbs/sec.	F_N lbs.	I_s[a] sec.	P_{oj}/P_1	I_s/I_N[*b]	C_D[c]
401	91.3	0.0057	0.64	107.5	2.98	2.37	0.756
401	102	0.0077	0.89	112.7	3.33	2.48	0.899
400	128	0.0098	1.11	110.9	4.20	2.45	0.903
399	159	0.0116	1.35	115.5	5.23	2.55	0.845
401	178	0.0144	1.69	116.7	5.94	2.53	0.929
393	186	0.0132	1.60	118.6	6.23	2.61	0.831
395	211	0.0152	1.79	115.7	7.10	2.55	0.839
399	246	0.0186	2.13	114.3	8.13	2.52	0.864
399	275	0.0223	2.51	111.9	9.24	2.47	0.923
389	309	0.0328	2.62	109.1	10.6	2.41	0.878
396	354	0.0268	2.94	109.1	11.8	2.41	0.851
411	387	0.0329	3.63	111.3	12.7	2.46	0.933
400	388	0.0298	3.22	106.7	12.8	2.36	0.862
395	413	0.0316	3.23	102.4	13.8	2.26	0.843
400	464	0.0356	3.69	102.7	15.4	2.27	0.836

Table II - continued

Injectant - CO_2 Orifice Diameter, d_j - ≈ 0.040 inches [d]

P_o psia	P_{oj} psia	$\dot{W}_j$ lbs/sec.	F_N lbs.	I_s [a] sec.	P_{oj}/P_1	I_s/I_s* [b]	C_D [c]
395	215	0.0056	0.68	118.9	7.19	2.63	-
399	277	0.0073	0.91	121.6	9.26	2.68	-
397	361	0.0096	1.16	118.8	11.6	2.62	-
398	398	0.0110	1.27	114.2	13.3	2.52	-
405	493	0.0141	1.65	114.5	16.7	2.5[illegible]	-

Table II - continued

Injectant - Ar Orifice Diameter, d_j - 0.0625 inches

P_o psia	P_{oj} psia	$\dot{W}_j$ lbs/sec.	F_N lbs.	I_s[a] sec.	P_{oj}/P_1	I_s/I_s^*[b]	C_D[c]
393	65.5	0.0028	0.37	127.1	2.22	2.84	0.498
392	74.7	0.0041	0.54	128.4	2.54	2.87	0.637
393	75.3	0.0042	0.52	119.4	2.55	2.67	0.646
389	84.8	0.0056	0.68	119.2	2.90	2.67	0.760
405	90.7	0.0059	0.76	122.8	3.03	2.75	0.769
391	101	0.0073	0.84	114.5	3.42	2.56	0.817
398	120	0.0091	1.12	120.0	4.02	2.69	0.870
391	123	0.0091	1.14	123.9	4.21	2.77	0.836
411	140	0.0101	1.32	127.1	4.63	2.84	0.836
398	158	0.0119	1.48	121.8	5.34	2.72	0.862
400	167	0.0129	1.55	120.8	5.62	2.70	0.862
399	184	0.0144	1.82	125.9	6.13	2.82	0.882
402	186	0.0134	1.72	122.0	6.24	2.73	0.854
405	221	0.0162	2.01	124.5	7.46	2.79	0.821
407	228	0.0171	2.08	119.9	7.64	2.68	0.855
404	228	0.0171	2.09	118.1	7.68	2.64	0.870
399	246	0.0189	2.28	121.0	8.22	2.71	0.862
399	285	0.0220	2.59	114.2	9.56	2.56	0.897
402	317	0.0255	3.04	116.8	10.5	2.66	0.907
404	347	0.0271	3.14	113.7	11.5	2.54	0.895
398	394	0.0303	3.42	112.1	13.3	2.51	0.870
400	409	0.0323	3.60	111.1	13.7	2.48	0.889
404	552	0.0434	4.21	97.6	18.4	2.18	0.880
406	680	0.0544	5.31	98.0	22.2	2.19	0.896
401	895	0.0721	6.51	91.5	29.9	2.05	0.885

Table II - continued

Injectant - N_2 Orifice Diameter, d_j - 0.0625 inches

P_o psia	P_{oj} psia	$\dot{W}_j$ lbs/sec.	F_N lbs.	I_s[a] sec.	P_{oj}/P_1	I_s/I_s*[b]	C_D[c]
393	110	0.0061	0.82	133.5	3.69	2.43	0.804
-	139	0.0080	1.08	129.3	4.68	2.36	0.858
397	171	0.0102	1.36	129.5	5.73	2.36	0.883
392	213	0.0127	1.70	130.1	7.16	2.37	0.878
397	266	0.0166	2.16	128.4	8.84	2.34	0.904
397	325	0.0200	2.46	121.9	10.9	2.22	0.890
391	440	0.0274	3.38	121.8	14.4	2.22	0.902
391	579	0.0349	4.19	117.4	19.5	2.14	0.883
398	709	0.0435	4.95	114.0	23.5	2.08	0.877
-	933	0.0579	6.26	108.6	31.4	1.98	0.886

Table II - continued

Injectant - He Orifice Diameter, d_j - 0.0625 inches

P_o psia	P_{oj} psia	$\dot{W}_j$ lbs/sec.	F_N lbs.	I_s[a] sec.	P_{oj}/P_1	I_s/I_s*[b]	C_D[c]
389	86.4	0.00173	0.53	297.4	2.93	2.13	0.748
395	88.2	0.00171	0.51	267.3	2.98	2.04	0.731
392	104	0.00224	0.66	283.5	3.51	2.01	0.812
462	120	0.00258	0.78	290.8	3.61	2.06	0.807
389	140	0.00318	1.01	307.7	4.79	2.18	0.851
389	159	0.00376	1.15	297.5	5.41	2.11	0.882
390	201	0.00472	1.41	289.5	6.85	2.05	0.879
393	242	0.00593	1.77	292.3	8.16	2.07	0.910
390	301	0.00726	2.18	293.1	10.2	2.08	0.896
393	365	0.0089	2.57	283.6	12.3	2.01	0.902
394	459	0.0110	3.03	272.8	15.0	1.93	0.879
409	656	0.0166	4.48	267.5	21.4	1.89	0.930
399	933	0.0224	5.97	265.6	31.9	1.88	0.875

Table II - continued

Injectant - He + Ar Orifice Diameter, d_j - 0.0625 inches

P_o psia	P_{oj} psia	$\dot{W}_j$ lbm/sec.	F_N lbs.	I_s^a sec.	P_{oj}/P_i	I_s/I_s^{*b}	C_D^c
398	90	0.0033	0.63	185.2	3.03	2.20	0.800
395	113	0.0044	0.86	190.2	3.90	2.25	0.829
403	136	0.0055	1.07	192.2	4.53	2.28	0.866
402	178	0.0072	1.35	187.0	5.96	2.22	0.859
404	225	0.0098	1.82	184.3	7.42	2.18	0.931
403	307	0.0136	2.50	183.3	10.2	2.17	0.943
403	432	0.0181	3.09	170.3	14.3	2.02	0.895
402	553	0.0242	3.95	164.1	18.4	1.94	0.925
401	709	0.0303	4.83	160.4	21.5	1.90	0.903
400	906	0.0394	6.18	157.9	30.2	1.87	0.919

Table II - continued

Injectant - H_2 Orifice Diameter, d_j = 0.0625 inches

P_o psia	P_{oj} psia	$\dot{W}_j$ lbs/sec.	F_N lbs.	I_s[a] sec.	P_{oj}/P_1	I_s/I_s*[b]	C_D[c]
402	101	0.00170	0.82	478.6	2.88	2.34	0.899
394	123	0.00226	1.08	476.5	4.17	2.33	0.963
395	176	0.00316	1.47	461.8	5.95	2.26	0.955
412	235	0.0042	1.88	453.4	7.66	2.21	0.947
401	342	0.00652	2.67	411.5	11.5	2.01	0.996
401	444	0.0083	3.45	419	14.9	2.05	0.975
396	599	0.0119	4.71	398.5	19.7	1.95	1.038
401	867	0.0157	6.22	399	29.1	1.95	0.947

a. I_s reduced to 70°F by: $I_s = (F_N/\dot{W}_j)(530/T_{oj})^{1/2}$

b. See Eq. (7) for definition of I_s^*.

c. $C_D = \dfrac{\dot{W}_j (T_{oj})^{1/2}}{A_j P_{oj} \left(\frac{\gamma}{g_o} \frac{g}{R}\right)^{1/2}} \phi^*$, where $\phi^* = 1 - 0.00776\ (P_{oj}/T_{oj}) + 26993\ (P_{oj}/T_{oj}^3)$ is a compressibility correction (18) used for CO_2 data ($\phi^* = 1$, for the other gases).

d. 0.0625 inch diameter orifice partially plugged with solder; exact diameter unknown.

Table III

Some Properties of the Injectants Used in Secondary Gas Injection Studies

GAS	$\mathcal{M}_j$	γ_j	I_s^* (sec)
CO_2	44.01	1.30	45.3
N_2	28.02	1.40	54.9
Ar	39.91	1.67	44.7
0.8 He + 0.2 Ar[a]	11.18	1.67	84.4
He	4.00	1.67	141.2
H_2	2.02	1.40	204.8

[a] Mole fractions

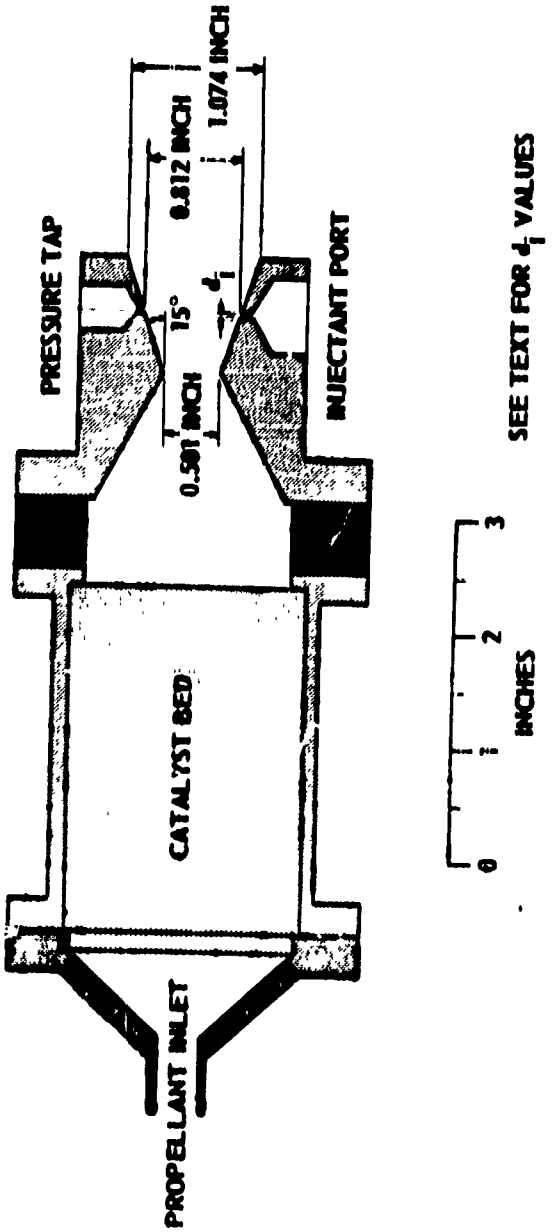

Fig. 1 RESEARCH ROCKET MOTOR USED IN SECONDARY GAS INJECTION EXPERIMENTS

The Johns Hopkins University
APPLIED PHYSICS LABORATORY
Silver Spring, Maryland

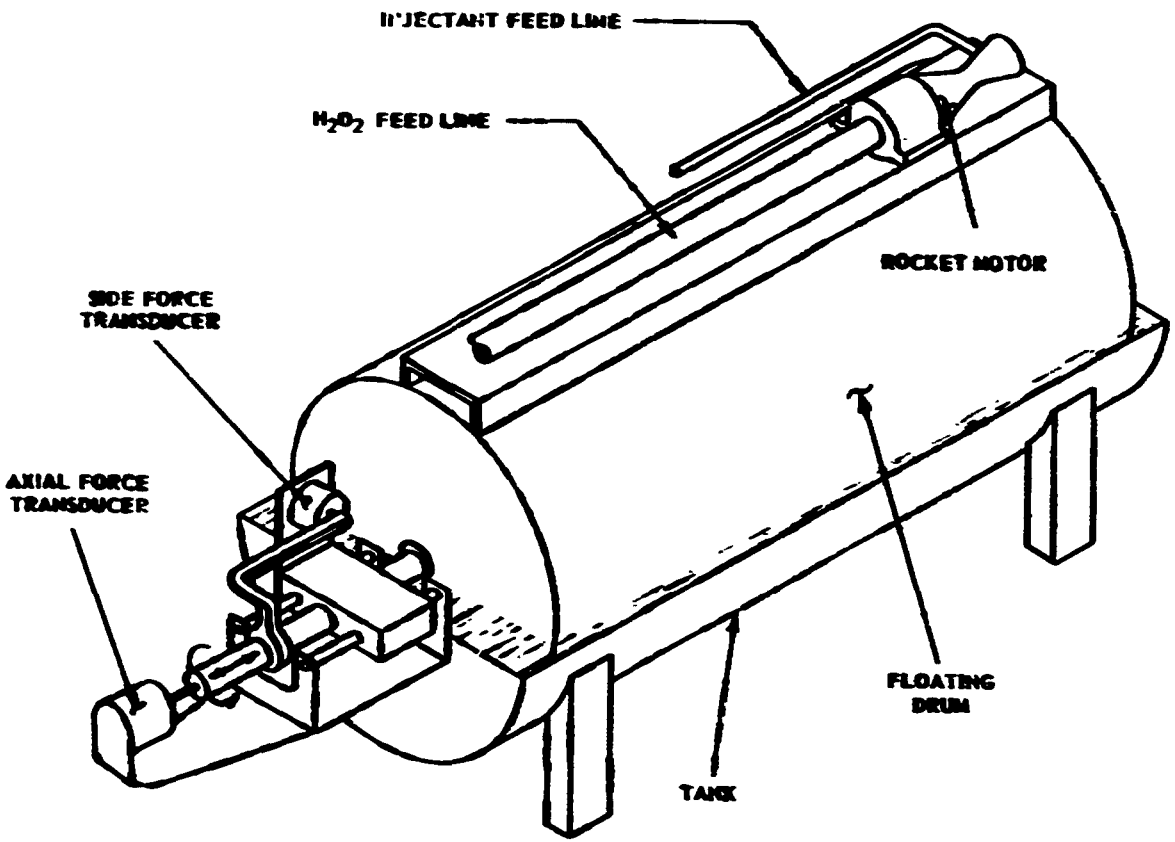

Fig. 2 GENERAL SETUP OF APPARATUS FOR SECONDARY GAS INJECTION EXPERIMENTS

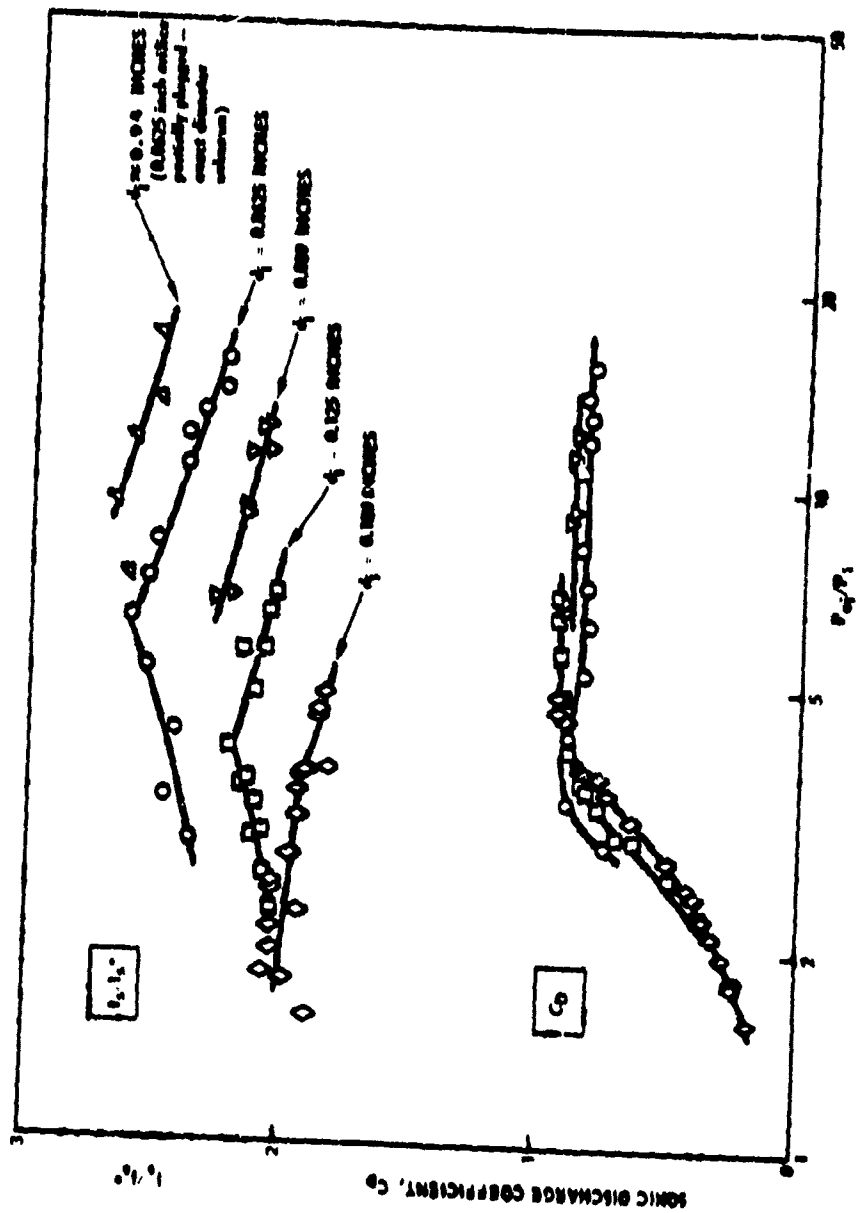

Fig. 3 EFFECT OF ORIFICE AREA ON SECONDARY GAS INJECTION (CO_2 INJECTANT AT 70°F)

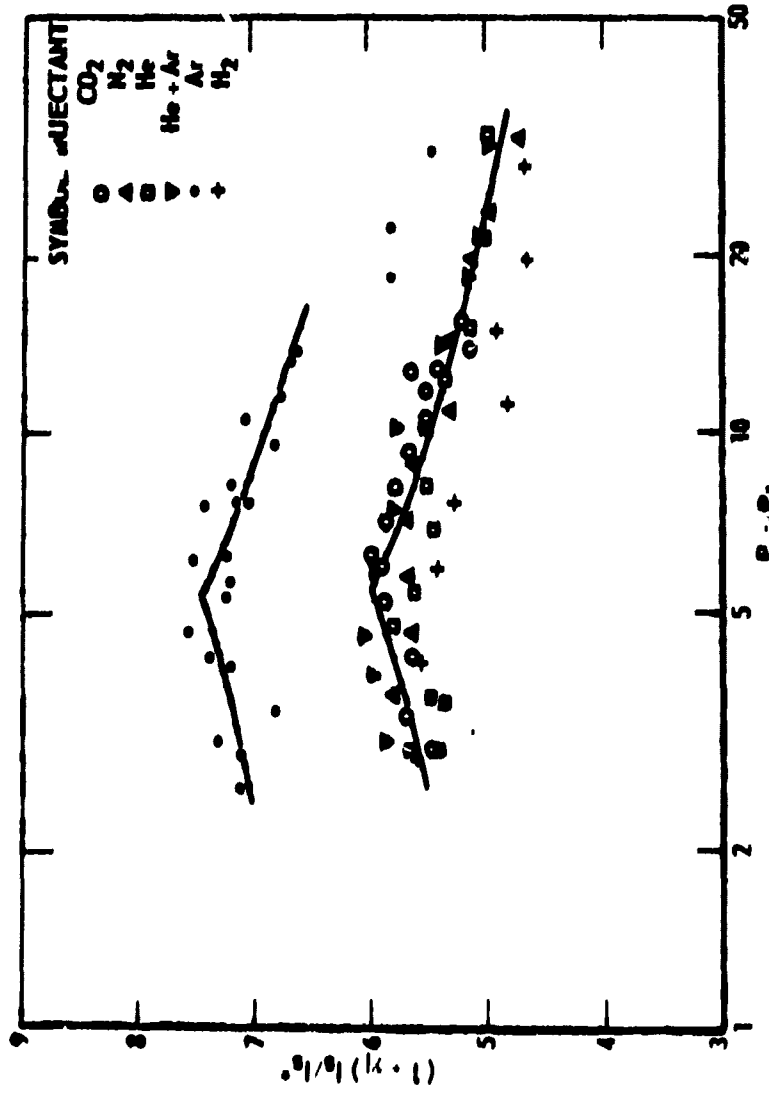

Fig. 4 CORRELATION OF SECONDARY INJECTION DATA FOR VARIOUS INJECTANT GASES (d_j = 0.0625 in., T_{oj} = 70°F)

The Johns Hopkins University
APPLIED PHYSICS LABORATORY
Silver Spring, Maryland

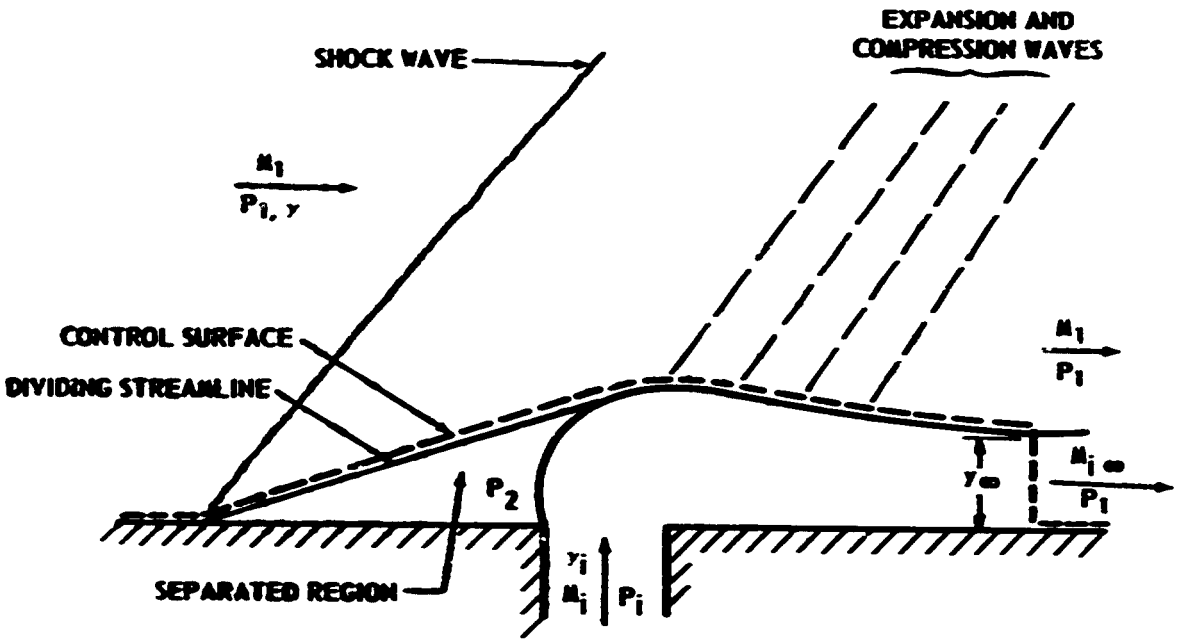

Fig. 5 SECONDARY GAS INJECTION MODEL

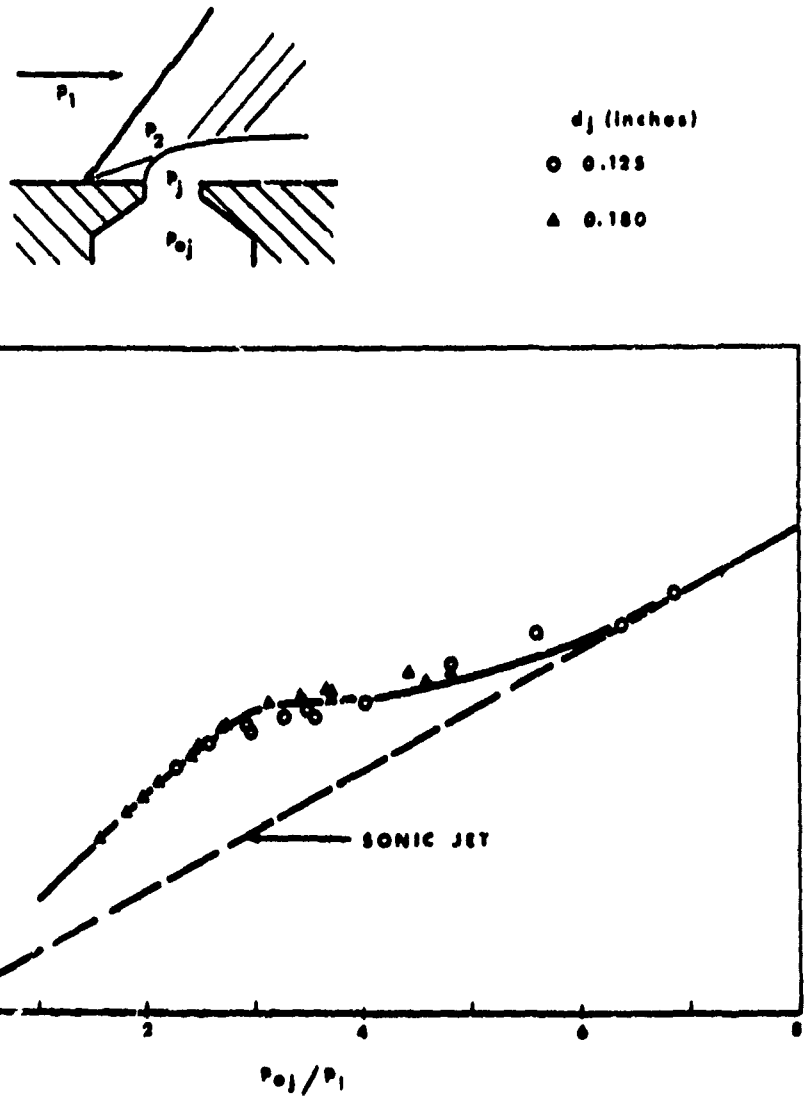

Fig. 6 APPROXIMATE PRESSURE RISE DUE TO INDUCED SHOCK WAVE (SUBSONIC CO_2 INJECTION DATA)

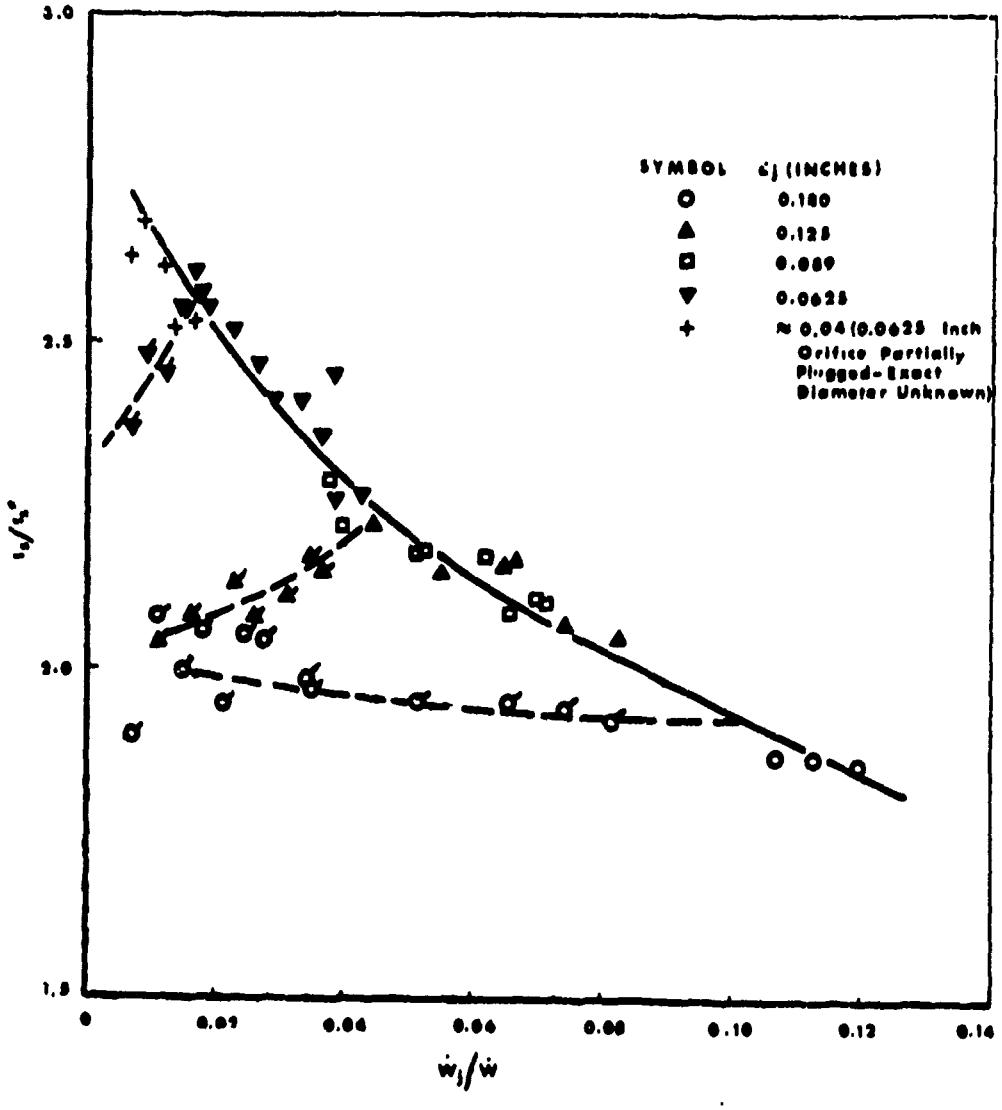

Fig. 7 CORRELATION OF SONIC SECONDARY INJECTION DATA [CO_2 INJECTANT AT 70°F; ALL SUBSONIC INJECTION DATA (P_{o_j}/P_1 4.0) ARE FLAGGED]

REFERENCES

1. United Aircraft Corporation Report R-63143-24, Thrust Axis Control of Supersonic Nozzles by Airjet Shock Interference, by G. F. Hausmann, 2 May 1952.

2. WADD Technical Report 60-329, Interaction Effects of Side Jets Issuing From Flat Plates and Cylinders Alined With a Supersonic Stream, by J. L. Amick and P. B. Hayes, May 1960.

3. Liepman, H. P., "On the Use of Side-Jets as Control Devices," ARS Journal, Vol. 29, June 1959, pages 453-455.

4. NASA Technical Note D-649, Loads Induced on a Flat-Plate Wing by an Air Jet Exhausting Perpendicularly Through the Wing and Normal to a Free-Stream Flow of Mach Number 2.0, by J. J. Janos, March 1961.

5. NASA Technical Note D-580, Surface Pressure Distributions With a Sonic Jet Normal to Adjacent Flat Surfaces at Mach 2.92 to 6.4, by R. W. Cubbison, B. H. Anderson, and J. J. Ward, February 1961.

6. NASA Technical Note D-743, Aerodynamic Interaction Effects Ahead of a Sonic Jet Exhausting Perpendicularly From a Flat Plate Into a Mach Number 6 Free Stream, by D. J. Romeo and J. R. Sterrett, April 1961.

7. University of Michigan, Department of Aeronautical Engineering, WTM-255, An Experimental Investigation of the Forces and Flow Field Produced by a Jet Exhausting Laterally From a Cone-Cylinder in a Mach 2.84 Stream, by J. L. Amick, C. E. Bond, and H. P. Liepman, November 1955

8. NASA Memo 12-5-58W, Interaction Effects Produced by Jet Exhausting Laterally Near Base of Ogive-Cylinder Model in Supersonic Main Stream, by P. W. Vinson, J. L. Amick, and H. P. Liepman, February 1959.

9. University of Michigan CM-979, Jet Interference Experiments Employing Body-Alone and Body-Fin in Configurations at Supersonic Speeds, by C. F. Carvalho and P. B. Hays, December 1960.

10. United Aircraft Corporation Report R-0937-33, Jet-Induced Thrust-Vector Control Applied to Nozzles Having Large Expansion Ratios, by A. Lingen, March 1957.

11. NAVORD Report 5904, Vol. II, A Theoretical and Experimental Investigation of a Method of Thrust Vector Control for Solid Rocket Motors, by G. H. Parker and S. Edwards, December 1959.

12. NASA Technical Memorandum X-416, A Cold Flow Investigation of Jet-Induced Thrust-Vector Control, by J. E. McAulay and A. J. Pavli, December 1960.

13. Bulletin of the 17th Meeting, JANAF-ARPA-NASA Solid Propellant Group, Vol. III, An Experimental Investigation of Jet-Induced Thrust Vector Control Methods, by C. J. Rodriguez, May 1961.

14. Bulletin of the 17th Meeting, JANAF-ARPA-NASA Solid Propellant Group, Vol. III, Propellant Gas Injection for Thrust Vector Control of Solid Propellant Rockets, by D. G. Drewry, B. T. Hnatiuk, T. E. Kallmeyer, H. D. Harmoning, D. P. Hanley and D. P. Hug, May 1961.

15. Paper presented at Fifth Symposium on Aeroballistics at U. S. Naval Ordnance Laboratory, Research on Secondary Injection for Thrust Vector Control Applications, by R. O. Slates, R. J. Geres, C. B. Benham, and D. F. Johnson, 16-18 October 1961.

16. ARS preprint No 2216-61 of paper presented at ARS Space Flight Report to the Nation, New York Coliseum, An Experimental Investigation of Shock Vector Control With Gaseous Secondary Injection, by A. J. Chamay and R. A. Sederquist, 9-15 October 1961.

17. JHU/APL Bumblebee Report No. 286, Interference Between a Jet Issuing Laterally From a Body and the Enveloping Supersonic Stream, by C. Ferrari, April 1959.

18. Jain-Ming Wu, R. L. Chapkis, and A. Mager, "Approximate Analysis of Thrust Vector Control by Fluid Injection," ARS Journal, Vol. 31, pages 1677-1685.

19. ARS preprint No. 2335-62 of paper presented at ARS Solid Propellant Rocket Conference, Baylor University, An Analysis of Gaseous Secondary Injection Into Rocket Nozzles, by E. J. Morgan, 24-26 January 1962.

20. Becco Research and Development Department Bulletin No. 67, Hydrogen Peroxide Physical Properties Data Book, 1955.

21. NACA Report 959, One-Dimensional Flows of an Imperfect Diatomic Gas, by A. J. Eggers, Jr., 1950.

22. Fairchild Engine and Airplane Corporation for Project SQUID (ONR), Contract No. NR 1858(25) NR-098-038, Exploratory Studies of Combustion in Supersonic Flow, by W. Chinitz and R. A. Gross, June 1959.

23. Shapiro, A. H., The Dynamics and Thermodynamics of Compressible Fluid Flow, The Ronald Press Co., New York, 1953.

24. NACA Report 1356, Investigation of Separated Flow in Supersonic and Subsonic Streams with Emphasis on Transition, by D. R. Chapman, D. M. Kuehn, and H. K. Larson, 1958.

25. Bulletin of the 17th Meeting, JANAF-ARPA-NASA Solid Propellant Group, Vol. II, Parameters Controlling the Performance of Secondary Injection, by C. B. Benham and C. J. Green, May 1961.

ACKNOWLEDGEMENTS

The authors would like to express their appreciation to E. Schmidt and J. Loveless of the APL/JHU High Temperature Laboratory for their assistance in the Laboratory, to I. Soslow for preparation of drawings and figures, and to R. H. Cramer for his continuing interest during the course of this investigation.

The technical papers and progress reports issued by APL in the CM series are characterized by extensive treatment of their subjects. Official Laboratory review of CM reports substantiates their technical validity and establishes suitability for distribution to qualified personnel outside Section T.

In addition to internal (Section T) distribution, initial distribution of CM-1010 has been made in accordance with Guided Missile Technical Information Distribution List MML 200/23, List No. 23, dated 3 April 1961.